Can. J. Remote Sensing, Vol. 32, No. 4, pp. 300–313, 2006

Multipolarized radar for delineating within-field variability in corn and wheat

A.M. Smith, P.R. Eddy, J. Bugden-Storie, E. Pattey, H. McNairn, M. Nolin, I. Perron, M. Hinther, J. Miller, and D. Haboudane

Abstract. In agriculture, there is growing interest in determining field spatial variability for implementing differential management practices, which should generate economic and environmental benefits. To date, the majority of studies involving remote sensing and differential management have focused on optical sensor systems. Less attention has been paid to synthetic aperture radar (SAR), despite the advantages of "all-weather" acquisition enabling information to be collected under cloud cover. This study examined the information content of multipolarization (HH, HV, VV, RR, LL, RL), multitemporal, and multiangle radar for delineating within-field spatial variability. On three dates in 2001, airborne C-band SAR data (35° and 55° incident angles) were acquired over four experimental fields. A series of fuzzy K-means analyses showed that the ability to differentiate zones was dependent upon the crop, the date in the growing season, and the pedodiversity of the field. Consistent with the soil and plant biophysical data, two of the four fields showed no spatial variability in radar backscatter. In the high-pedodiversity cornfield (*Zea mays* L.), three zones of productivity were discriminated early in the growing season and two zones of productivity in mid-season. Late in the season as a result of saturation of the radar signal, no spatial variability was evident. In corn, the results were similar regardless of the radar polarization. In the wheat (*Triticum aestivum* L.) field, which was of lower pedodiversity, two zones were identified in early-, mid-, and late-season images. Differences were evident among polarizations, with VV and HV being most sensitive to within-field variation. The delineated zones in both fields were shown to relate to plant and soil parameters, suggesting that radar may be a valuable tool in delineating spatial variation in producer fields and delineating differential management units.

Résumé. La détermination de la variabilité spatiale des champs soulève de plus en plus d'intérêt en l'agriculture, pour mettre en application des pratiques de gestion agricole différentielles, pouvant produire des avantages économiques et écologiques. Jusqu'à maintenant, la majorité des études impliquant la télédétection et la gestion différentielle se sont concentrées sur les systèmes de télédétection optique. Le radar à antenne synthétique (SAR) a suscité moins d'attention en dépit de sa capacité d'acquisition en « tous temps » qui permet de recueillir l'information sous couverture nuageuse. Cette étude examine la teneur en information de la multi-polarisation (HH, HT, VV, RR, LL, RL) radar, de son acquisition multi-temporelle et multi-angulaire afin de délimiter la variabilité spatiale des champs. En 2001, des données du SAR en bande C (à 35° et 55° d'angles d'incidence) ont été acquises par avion sur quatre champs expérimentaux à trois dates différentes. Une série d'analyses de k-moyennes flou a montré que la capacité de différencier des zones variait selon les cultures, la date d'acquisition dans la saison de croissance et la pédodiversité du champ. En accord avec les données biophysiques du sol et des plantes, deux des quatre champs n'a montré aucune variabilité spatiale dans le signal rétrodiffusé de radar. Dans le champ de maïs à pédodiversité élevée (*Zea mays* L.), trois zones de productivité ont été distinguées tôt en saison de croissance et deux zones de productivité ont été identifiées en pleine saison. Plus tard en saison, aucune variabilité spatiale n'était ressortie en raison de la saturation du signal de radar. Dans le maïs, les résultats étaient semblables indépendamment de la polarisation du radar. Dans le champ de blé (*Triticum aestivum* L.), qui avait une pédodiversité moindre, deux zones ont été identifiées dans les images acquises en début, milieu et fin de saison. Les différences étaient évidentes parmi des polarisations avec VV et la polarisation HV, qui était la plus sensible aux variations à l'intérieur du champ. Les zones délimitées dans les deux champs se sont avérées être liées aux paramètres de la plante et du sol suggérant que le radar pourrait être un outil valable de délimitation de la variation spatiale des champs agricoles et de des unités différentielles de gestion.

Received 18 October 2005. Accepted 5 September 2006.

A.M. Smith[1] and P.R. Eddy. Lethbridge Research Centre, Agriculture and Agri-Food Canada, 5403-1st Avenue South, Lethbridge, AB T1J 4B1, Canada.

J. Bugden-Storie, E. Pattey, H. McNairn, and M. Hinther. Environmental Health, Agriculture and Agri-Food Canada, 960 Carling Avenue, Ottawa, ON K1A 0C6, Canada.

M. Nolin and I. Perron. Soils and Crops Research and Development Centre, Agriculture and Agri-Food Canada, 979 de Bourgogne Avenue, Sainte-Foy, QC G1W 2L4, Canada.

J. Miller. York University, 4700 Keele Street, Toronto, ON M3J 1P3, Canada.

D. Haboudane. Université du Québec à Chicoutimi (UQAC), 555, boulevard de l'Université, Chicoutimi, QC G7H 2B1, Canada.

[1]Corresponding author (e-mail: smitha@agr.gc.ca).

Introduction

Site-specific or precision agriculture aims to manage within-field spatial variability by optimizing the placement of seed, fertilizer, and pesticide inputs (Pierce and Nowak, 1999) with regard to sound agronomical principles for both economic gain and environmental sustainability. This could involve increasing inputs on poorer yielding areas of the field or it may mean taking the inputs from the poorer yielding areas and adding them to the higher yielding areas to maximize production (Lu et al., 1997). The development of enabling technologies, including variable-rate applicators, global position systems (GPS), yield monitors, geographic information systems (GIS), and remote sensing, provides powerful tools for site-specific agriculture (Stafford, 2000). Remote sensing offers a nondestructive, noninvasive means of acquiring pre-season, in-season, or post-season field information. This information includes mapping spatial variation that is quasi-static (e.g., soil based) and dynamic (e.g., weather driven) (Moran et al., 1997; Brisco et al., 1998). The remote sensing imagery available from IKONOS, QuickBird, SPOT, Landsat, and RADARSAT satellites provides very large scale measurements (1–25 m resolution). In practical terms given the size of farm machinery, however, land management decisions are made on a much smaller scale than that provided by the imagery. Management zones, which are defined as areas of the field "that express homogeneous combinations of yield limiting factors for which a single rate of a specific crop input is appropriate" (Doerge, 1999), appear to be the most practical way of implementing site-specific agriculture.

To date, the majority of studies involving remote sensing and site-specific agriculture have focused on optical sensor systems (Frazier et al., 1997; Mulla and Schepers, 1997; Fleming et al., 2000; McNairn et al., 2001; Mulla et al., 2001; Morgenthaler et al., 2003; Seelan et al., 2003; Liu et al., 2005). The delineation of homogeneous zones (HZ) using optical data depends on the exploitation of the differential reflectance properties among soils (Chen et al., 2000) and crops (Yang and Anderson, 2000). Soil and crop conditions vary dynamically. Thus, remote sensing data must be acquired in a timely fashion. In the case of optical sensors, cloud cover often limits timely acquisitions and hinders the implementation of this technology in site-specific agriculture.

Less attention has focused on synthetic aperture radar (SAR) despite the advantages of "all-weather" acquisition capabilities enabling information to be collected regardless of cloud cover. This advantage is especially suitable in the spring during crop emergence and rapid growth. Further, SAR has full diurnal collection capability due to its independence from solar illumination. The availability of only a limited number of SAR satellite sensors, with single-frequency and single-polarization capability, has impeded the uptake and implementation of radar within some user communities. The complexity of the interactions of microwaves with agricultural targets has also been a challenge to users attempting to apply this technology within soil and crop studies. Knowledge within the agricultural community with respect to the exploitation of radar is maturing, however, and access to multipolarization SAR imagery from space is beginning. For agricultural applications, single-channel radar images are of limited value unless they are combined in a multitemporal series (McNairn and Brisco, 2004; van der Sanden, 2004). The next generation of SAR satellite sensors, including ENVISAT ASAR (C-band with dual-polarization capability), RADARSAT-2 (C-band fully polarimetric), and ALOS PALSAR (L-band fully polarimetric), holds significant promise for soil and vegetation applications (van der Sanden, 2004).

For agricultural targets, radar backscatter primarily responds to soil moisture, soil surface roughness, and vegetation architecture. Some of the complexities in the interpretation can be mitigated by prior knowledge of crop type, tillage practices, row direction, soil type, topography, and planting date, much of which is constant or known within an agricultural field (Moran et al., 1997). In the context of site-specific agriculture, limited studies to date suggest that multipolarization radar could provide valuable and timely information with respect to delineation of homogeneous zones (McNairn et al., 2002; 2004). Multipolarization refers to both linear and circular copolarized and cross-polarized radar. In linear polarized radar the tip of the electric field vector traces a straight line on a plane perpendicular to the direction of wave propagation. The copolarization (HH and VV) and cross-polarization (HV and VH) indicate if the wave was transmitted and (or) received in the horizontal (H) or vertical (V) plane. In circular polarization the tip of the electric field vector traces a circle in a plane perpendicular to the direction of the wave propagation and can be designated circular copolarization (RR or LL, where R represents right-handed circular and L represents left-handed circular) or cross-polarization (RL and LR) depending on the direction of rotation relative to the observed in the transmit and receive mode.

Within-field variability in radar backscatter can be attributed to differential soil descriptors during periods of low vegetation growth and to the differential growth and development of the crop itself at more advanced vegetation stages. In both studies by McNairn et al. (2002; 2004), only a single date and single incidence angle of SAR imagery were available, either early in the season or just prior to harvest. Early in the growing season, in fields planted to wheat, peas, and canola, differential zones derived using linear copolarized and cross-polarized C-band radar related well to differences in the height, density, and overall health of the plants (McNairn et al., 2002). In zones of greater density and taller plants, radar backscatter was lower than that for areas of shorter, less dense plants. At this early stage of growth, the crop canopy was still open and the underlying soils probably influenced the radar backscatter; the soils in the areas with higher density plants were drier (20%–40% volumetric moisture) than those in the poorer vegetation area (40%–60% volumetric moisture). In a similar study, an early season image acquired over a soybean field was delineated into three or four zones based on radar backscatter in VV, HV, and RL polarizations. The zones corresponded to

differential soil drainage and crop emergence (McNairn et al., 2000). The ability to differentiate zones of productivity in soybean and corn fields decreased as the crops matured due to saturation of the radar signals, but in wheat fields the ability to differentiate zones of productivity increased as the crop matured (McNairn et al., 2000; 2004). In both of these studies, the patterns that emerged could be related to soil variability over the field that directly influenced the wheat canopy.

The availability of data from more advanced SAR satellites and our increased understanding of the potential of multipolarization SAR have stimulated the research reported here. The objectives of this study were (*i*) to assess the potential of linear and circular polarized C-band SAR acquired at two incidence angles to define homogeneous within-field zones on three dates during the growing season, and (*ii*) to examine the relevance of these zones in terms of plant and soil biophysical descriptors. The inclusion of the multitemporal SAR data acquired at two incidence angles and also the crops corn and soybean in addition to wheat provided a new component relative to the studies of McNairn et al. (2002; 2004).

Methods

Study site

The study site was located in the Greenbelt farm area in Ottawa, Canada (45°19′N, 75°49′W). Four fields were selected for intensive study, with one field planted to soybean (*Glycine max* L.) (F_{16}), two fields to corn (*Zea mays* L.) (F_{13} and F_{23}), and one field to wheat (*Triticum aestivum* L.) (F_{25}). In each of the fields, soil and crop biophysical descriptors were collected from preselected 20 m × 20 m areas at the time of the airborne C-band SAR data acquisitions. The sampling sites were selected to represent within-field features that could influence yield. There were three sampling sites in F_{16}, two sampling sites in F_{13} (later planted corn), four sampling sites in F_{23} (earlier planted corn), and seven sampling sites in F_{25}. The descriptors collected included phenological stage, height, biomass, leaf area index (LAI), soil roughness, and soil moisture. Field-scale maps of LAI derived from compact airborne spectrographic imager (CASI) imagery (Haboudane et al., 2004) and soil electrical conductivity (EC) at 0–30 and 0–100 cm measured using the VERIS 3100 technology (Perron et al., 2003) and of yield derived from yield monitor data were also available for comparison with the SAR data. The yield monitor on a combine provides a direct measure of the weight and humidity of grains per unit area, georeferenced when used in combination with a GPS during crop harvesting.

SAR data acquisition

Airborne C-band (5.66 cm) polarimetric data were acquired three times during the 2001 growing season using the Convair CV-580 operated by Environment Canada. The dates of the three intensive field campaigns (IFC) included 13 June (IFC_1), 26 June (IFC_2), and 19 July (IFC_3). The single-look complex data, acquired at two incident angles (35° and 55°), were recorded at a pixel spacing of 4.0 m (slant range) by 0.4 m (azimuth). Problems with the antenna initialization resulted in the 35° data for IFC_2 being discarded.

Polarimetric active radar calibrators and corner reflectors were deployed at the study site on all three acquisition dates. The information from these instruments was used in the radiometric calibration of the SAR data. Polarimetric processing and radiometric calibration were completed by the Canada Centre for Remote Sensing (CCRS). The within-scene calibration accuracy was 0.8 dB in intensity and 10° in phase (Hawkins et al., 1999). The radiometrically calibrated data were geometrically corrected by CCRS to provide a ground-range product containing georeferenced pixels of 4 m spatial resolution (both azimuth and range). Products synthesized from the complex data included HH, HV, and VV linear and RR, RL, and LL circular transmit–receive polarization images. The data were delivered as 32-bit power (σ^o) images. The SAR images were resampled from 4 to 10 m resolution using cubic convolution to match the lowest resolution data available from the yield monitor. This resampling also served to reduce the speckle inherent in radar images. SAR data quality was assessed using the approach presented in Budgen et al. (2003).

SAR image analysis

Visual examination of the SAR imagery revealed that, regardless of the date of acquisition, there was no spatial variability in backscatter across F_{13} and F_{16}. These two fields showed no variability in plant biophysical descriptors (data not shown), nor in the soil descriptors as shown in the soil survey map of the Ottawa urban fringe (Marshall et al., 1979). Conversely, variability was evident in the radar backscatter, the ground-sampled plant biophysical descriptors, and the soil survey map for fields F_{23} and F_{25}. Thus, the analysis was confined to F_{23} and F_{25}. The SAR imagery for each field was subset using perimeter vectors created from differential GPS measurements.

Preliminary examination of the data involved extracting the mean radar backscatter in power (σ^o) for F_{23} and F_{25} to determine the seasonal trajectory for each polarization. The data are presented in decibels (dB). The relationship among the six different radar polarizations and the crop responses was also examined by extracting the backscatter values from each pixel in the image and conducting a series of correlation analyses (SAS Institute Inc., 1999).

To determine the ability to delineate homogeneous zones (HZs) with the various polarizations, the SAR image data for each date and incident angle were converted from units of power to amplitude and subjected to unsupervised classification. A series of unsupervised classifications involving the linear only (HH, HV, VV) and the linear plus circular (HH, HV, VV, RR, LL, RL) polarizations were performed using the fuzzy K-means algorithm with two to five classes inclusive. A 5 × 5 postclassification mode filter was applied to each classified image to remove isolated pixels. The reduction in variance of radar backscatter with class (Fridgen et

al., 2000) along with analyses of variance involving the radar backscatter values for each pixel in the various classes were used to assess the appropriate number of classes. To be considered significantly different, the difference in mean backscatter values between classes had to be in excess of the within-scene calibration accuracy of 0.8 dB. The reduction in total within-class radar backscatter variance as compared with radar backscatter observed on a whole-field basis was calculated as

$$\% \text{ of total variance} = 100 \times (S_T^2 / S_{WF}^2)$$

where S_{WF}^2 is the variance calculated from all observations for a given field, and S_T^2 is the summed weighted variance from the 1 to c individual classes being examined. The weighted variance in class c was calculated as

$$S^2c = \left[\frac{1}{n}\sum_{i=1}^{n_z}(Y_i - \overline{Y}c)^2\right]\left(\frac{n_z}{n_T}\right)$$

where n_z is the number of pixels in class c, n_T is the total number of pixels in the field, Y_i is the measured radar backscatter of the ith observation in class c, and $\overline{Y}c$ is the mean of all i radar backscatter observations in class c.

The relationship between the classes defined by radar backscatter and crop and soil descriptors was investigated using two levels of data, the sample site data and the field-level maps. With respect to the site data, the radar backscatter and class numbers were extracted from the 20 m × 20 m area (2 × 2 pixel window). Analyses of variance were used to assess significant differences between the plant descriptors, which included biomass, LAI, and height. With respect to the field-level data, a 50 m grid was overlaid on the various unsupervised images, the LAI, soil EC, and yield images, and a 2 × 2 pixel window was selected within each grid cell to limit colinearity between

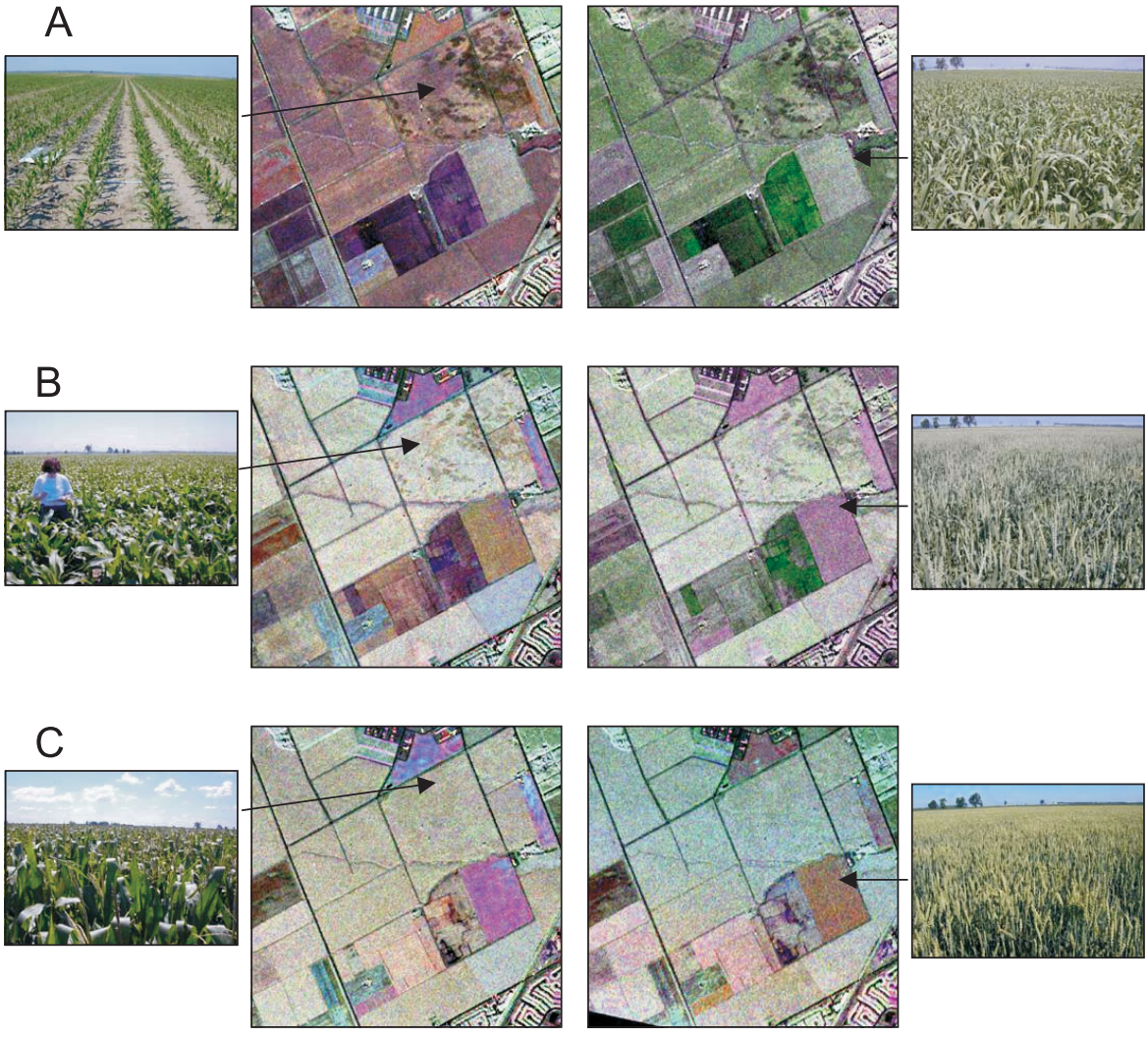

Figure 1. Colour composite images of linear HH–HV–VV (left) and circular RR–LL–RL (right) polarized radar images, acquired at 55° incident angle, in (A) IFC_1, (B) IFC_2, and (C) IFC_3. The stage of corn (F_{23}) growth is shown on the left, and that of wheat (F_{25}) on the right.

Table 1. The relationship between zone delineation using HH-polarized radar and corn biophysical descriptors measured at select sample sites on three different dates.

Sample site	LAI	Fresh biomass ($kg \cdot m^{-2}$)	Height (cm)	Zone	
				Incident angle 35°	Incident angle 55°
IFC_1					
1	0.087c	0.059c	23.2b	1	1
2	0.364b	0.335b	53.6a	2	3
3	0.527a	0.427a	57.3a	3	3
4	0.102c	0.058c	20.5b	1	2
SE	0.022	0.020	1.9		
IFC_2					
1	0.542c	0.447c	53.6c	—	1
2	1.811b	1.966b	91.3b	—	2
3	**2.217**a	2.722a	**113.9**a	—	2
4	0.596c	0.551c	40.0d	—	1
SE	0.111	0.100	2.3		
IFC_3					
1	**2.826**c	4.707b	**197.5**c	—	—
2	**3.249**b	5.219b	**237.0**b	—	—
3	**3.529**a	6.790a	**261.3**a	—	—
4	**2.606**c	3.839c	**177.8**d	—	—
SE	0.095	0.271	4.0		

Note: Means within a column followed by the same letter are not significantly different at $P = 0.05$. SE, standard error of the mean; —, no zone delineated. Values in bold exceed those known to cause saturation of the radar signal.

samples. The mode value for the class and the average for the various biophysical descriptors were calculated for each 2 × 2 pixel window. Fifty percent of these values were randomly selected to determine the relationship between class and the soil and plant descriptors. Analyses of variance were used to determine significant differences between the SAR backscatter derived classes and the LAI, soil EC, and yield (SAS Institute, Inc., 1999) from the field-level maps.

Results and discussion

Corn (F_{23})

Visual examination of the various SAR images showed spatial variation in the radar backscatter across F_{23} in IFC_1. The spatial patterns were less prominent mid-season in the IFC_2 images and absent from the IFC_3 images (**Figure 1**). This disappearance of within-field spatial variation in radar backscatter from corn later in the growing season is consistent with previous findings (McNairn et al., 2000). In IFC_3, the corn exceeded 1 m in height and the LAI was in excess of 2, both of which are reported to cause saturation of the radar signal (Ferrazzoli et al., 1997; McNairn et al., 2000). The biophysical data from the sampling sites indicated that in some areas of the field, the height and LAI of the corn canopy in IFC_2 exceeded these saturation values (**Table 1**). The mean radar backscatter

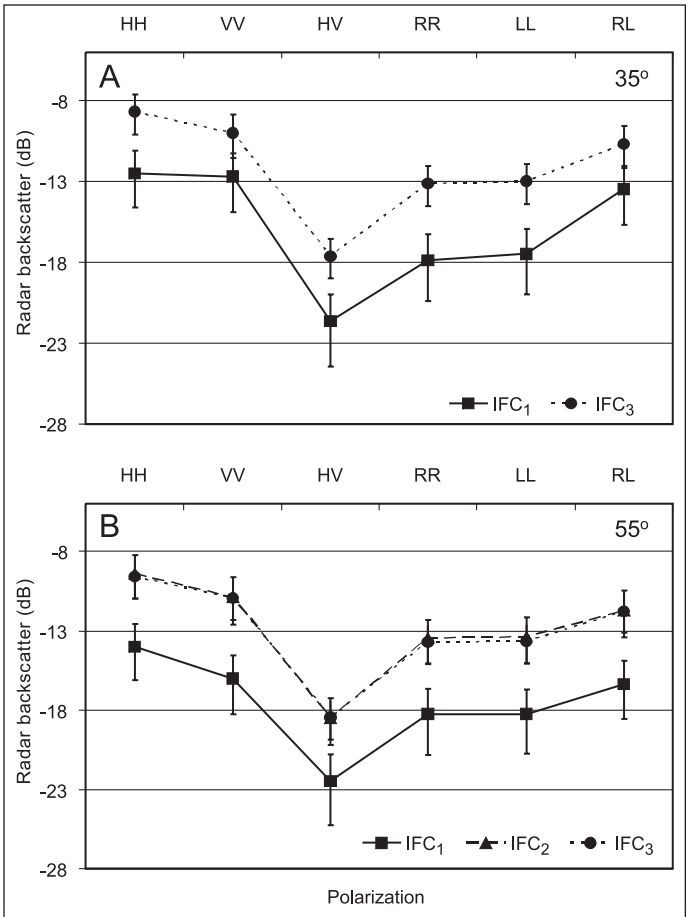

Figure 2. Seasonal changes in the C-band mean radar backscatter with its associated standard error (vertical bars) of corn in F_{23}: (A) 35° incident angle; (B) 55° incident angle.

values for F_{23} increased from IFC_1 to IFC_2. From IFC_2 to IFC_3 mean radar backscatter associated with all six polarizations did not increase, further supporting the suggestion that the radar signal was saturated by IFC_2 (**Figure 2**). The mean radar backscatter and visual examination of the spatial patterns in the images indicate that F_{23} responded similarly to the six different polarizations and the two incident angles. This is contrary to the study of McNairn et al. (2000), who reported that patterns of within-field spatial variability in corn were most pronounced in the linear cross-polarization (HV) and circular copolarization (RR). These polarizations are associated with multiple scattering or volume scattering from within the canopy.

The radar backscatter values for the six polarizations collected at the 55° incident angle were highly correlated with each other in IFC_1 (correlation coefficient r = 0.78–0.96) (**Table 2**). Radar backscatter values in the six polarizations in IFC_2 were also well correlated, although the correlation coefficients decreased. In IFC_3 regardless of incident angle, the correlations among radar backscatter values from the six polarizations were low. The exception was the correlation between linear-like polarizations (VV and HH) and the circular cross-polarization (RL). In IFC_1, the correlation among radar

backscatter values from images acquired at the 35° incident angle was only strong for select polarizations: RL was highly correlated with HH or VV (r = 0.89–0.94), and RR and LL were well correlated with HV (r = 0.92–0.94) (**Table 3**). Linear-like polarizations (HH and VV) and circular cross-polarizations (RL and LR) are associated with single-bounce scattering events. To record a significant response for linear cross-polarizations (HV and VH) and circular-like polarizations (RR and LL), multiple or volume scattering must occur such that the incident wave is repolarized into the orthogonal polarization. In reality, the response is usually the result of a number of scattering mechanisms from the target, but often with a single scattering mechanism dominating. The implication of the high correlation between the linear and circular polarizations at the early corn growth stages is that fewer polarizations should be required to assess the within-field variability.

The fuzzy K-means classifications support this observation, as the derived homogeneous zone (HZ) maps were similar for all polarizations and combinations of polarizations. With respect to HH, regardless of incident angle, the field could be delineated into three HZs using the IFC_1 images. The reduction in variance of HH backscatter was 55% and 70% for the 35° and 55° incident angles, respectively (**Figure 3**). The mean backscatter values for the three HZs were significantly different from one another: HZ_1 had the lowest value, HZ_2 had an intermediate value, and HZ_3 had the highest value. In each case, the differences in the mean radar backscatter values among the HZs (0.93–2.09 dB for the 35° incident angle and 1.62–2.61 dB for the 55° incident angle) were greater than the within-scene calibration accuracy of 0.8 dB (**Table 4**). In IFC_2, only two HZs were defined, based on the reduction in variance of HH backscatter and the difference in mean backscatter between HZs (0.98 dB). The 30% reduction in variance of HH backscatter in IFC_2 was less than that in IFC_1, but the mean backscatter values for each HZ were substantially greater (–9 dB compared with –13 to –15 dB). Growth of the corn and higher biomass in IFC_2 compared with IFC_1 would account for this increase in backscatter. Saturation of the signal in certain locations of the field likely occurred and reduced the number of HZs that could be delineated in F_{23}.

The HZs generated using the single HH polarization were compared with the HZs generated from the other single polarizations (VV or HV) and the HZs generated when all linear polarizations were combined, or when all linear and circular polarizations were combined. Visually, no marked differences were observed. For all single polarizations and polarization combinations, delineation into three HZs was appropriate based on the radar backscatter variance reduction and mean backscatter for the HZs early in the season (IFC_1). Later in the season, two HZs were appropriate (IFC_2). The number of pixels, expressed as a percentage, classified in a different zone ranged from only 3% to 25% (**Table 5**) among the classifications derived using the various polarizations. Visual examination of the classified images indicates that, in general, the pattern of the HZ zones is similar and that the differences can be attributed primarily to changes in the HZ boundaries rather than to discrete changes in the HZs.

Table 2. Correlations (r) between C-band linear and circular copolarized and cross-polarized radar backscatter from corn (F_{23}) for the image acquired at the 55° incident angle.

	HH	VV	HV	RR	LL	RL
IFC_1						
HH		**0.78**	**0.84**	**0.88**	**0.93**	**0.96**
VV			**0.87**	**0.85**	**0.84**	**0.91**
HV				**0.96**	**0.94**	**0.87**
RR					**0.92**	**0.88**
LL						**0.90**
RL						
IFC_2						
HH		**0.72**	**0.72**	**0.78**	**0.71**	**0.91**
VV			**0.70**	**0.83**	**0.72**	**0.91**
HV				**0.81**	**0.75**	**0.75**
RR					0.69	**0.80**
LL						0.67
RL						
IFC_3						
HH		0.48	0.28	0.44	0.32	**0.84**
VV			0.17	0.30	0.28	**0.81**
HV				0.49	0.59	0.21
RR					0.34	0.25
LL						ns
RL						

Note: Significance values above the user-defined threshold of 0.70 are in bold. ns, not significant correlations at P = 0.05.

Table 3. Correlations (r) between C-band linear and circular copolarized and cross-polarized radar backscatter from corn (F_{23}) for the image acquired at the 35° incident angle.

	HH	VV	HV	RR	LL	RL
IFC_1						
HH		**0.78**	0.23	0.32	0.35	**0.94**
VV			0.35	0.39	0.38	**0.89**
HV				**0.94**	**0.92**	ns
RR					**0.85**	ns
LL						0.17
RL						
IFC_3						
HH		0.36	0.25	0.58	**0.76**	0.91
VV			0.25	0.18	0.40	0.65
HV				0.36	0.55	0.27
RR					0.50	0.39
LL						0.65
RL						

Note: Significance values above the user-defined threshold of 0.70 are in bold. ns, not significant correlations at P = 0.05.

Table 4. Mean (±SE) backscatter values (dB) for the zones in the cornfield (F_{23}) derived from HH-polarized radar.

Zone	IFC_1 (35°)	IFC_1 (55°)	IFC_2 (55°)
1	–14.5±0.2c	–16.6±0.2c	–10.0±0.1b
2	–12.4±0.2b	–14.0±0.1b	–9.0±0.1a
3	–11.5±0.1a	–12.4±0.1a	—

Note: Means within a column followed by the same letter are not significantly different at $P = 0.05$.

In terms of soil and crop biophysical descriptors, the HZs identified on the basis of radar backscatter appear to relate to both soil types and crop productivity. Given the similarity in the HZs derived using the various polarizations and combinations of polarizations, only the results for HH are discussed. Visual observation shows that in IFC_1 and IFC_2 the differential patterns evident in the classified images relate to differential soil types identified in the detailed soil survey map of the Ottawa urban fringe (Marshall et al., 1979). HZ_1 in both the IFC_1 and IFC_2 images, characterized by lower backscatter, is primarily an area of medium- to fine-grained, well-drained,

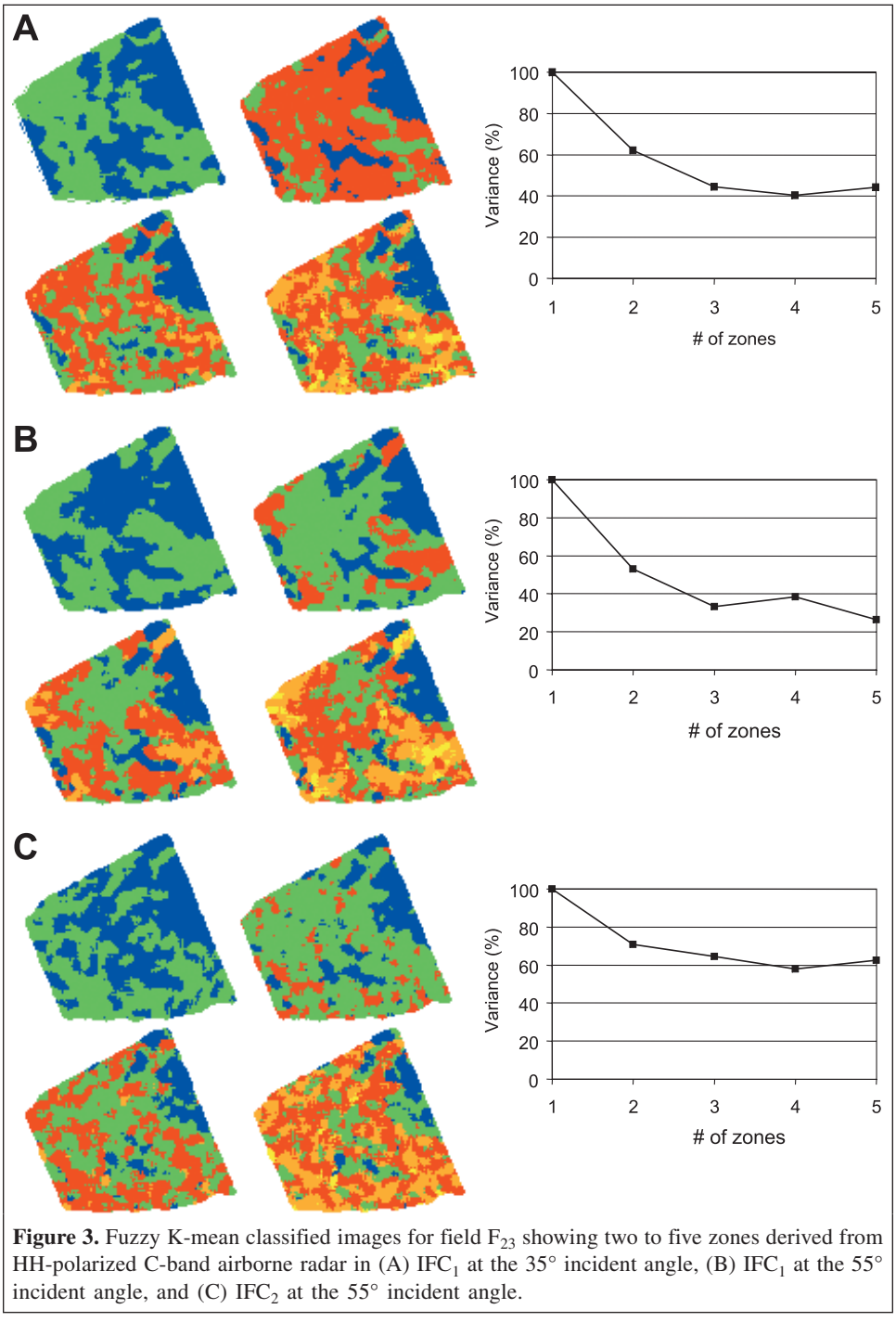

Figure 3. Fuzzy K-mean classified images for field F_{23} showing two to five zones derived from HH-polarized C-band airborne radar in (A) IFC_1 at the 35° incident angle, (B) IFC_1 at the 55° incident angle, and (C) IFC_2 at the 55° incident angle.

Table 5. The difference in per pixel classification for the cornfield (F_{23}) using different polarizations and polarization combinations relative to HH polarization alone.

Field campaign	Incident angle (°)	Zone	Difference in the number of pixels classified in a different zone (%)						
			VV	HV	HH+VV	HH+HV	HV+VV	HH+HV+VV	L+C[a]
IFC_1	35	3	23.5	24.5	15.6	4.9	23.9	15.4	16.7
IFC_1	55	3	22.4	21.7	8.9	3.9	20.8	9.8	10.7
IFC_2	55	2	23.9	24.7	15.6	3.0	24.7	16.2	17.2

[a]Linear (HH, HV, VV) plus circular (RR, RL, LL) polarizations.

Table 6. Relationship between zone delineation using HH-polarized radar and soil electrical conductivity (EC_{30} and EC_{100}) and field-scale corn biophysical descriptors (F_{23}).

Field campaign	Incident angle (°)	Zone	EC_{30} (mS)	EC_{100} (mS)	LAI[a]	Yield ($kg \cdot m^{-2}$)
IFC_1	35	1	2.88±0.64c	6.71±1.11b	0.25±0.01c	6.28±0.12b
		2	7.54±0.87b	16.89±0.69a	0.30±0.01b	7.28±0.12a
		3	9.38±0.83a	20.12±1.43a	0.34±0.02a	6.78±0.256ab
IFC_1	55	1	2.40±0.66b	5.56±1.06b	0.24±0.01c	6.22±0.18b
		2	8.79±0.43a	18.81±0.70a	0.29±0.01b	7.23±0.12a
		3	9.30±0.75a	20.33±1.22a	0.36±0.01a	6.59±0.20b
IFC_2	55	1	6.16±0.54b	13.79±0.95b	1.75±0.10b	6.72±0.14b
		2	8.64±0.57a	18.23±1.00a	2.27±0.11a	7.10±0.15a

Note: Means within each field campaign in each column followed by the same letter are not significantly different at $P = 0.05$.

[a]Derived from CASI measurements.

sandy soils, whereas HZ_2 and HZ_3 are areas of poorly drained soils developed from strongly acidic, coarse- or fine-textured marine modified material (see Figure 1 and Table 1 in Liu et al., 2005).

The corn height, biomass, and LAI in IFC_1 and IFC_2 were significantly higher at sampling site 3 than at any other sampling site and significantly lower at sites 1 and 4 than at sites 2 and 3 (**Table 1**). At both incident angles, the higher productivity sampling site 3 was located in the HZ exhibiting the highest backscatter, intermediate productivity sampling site 2 was located in the HZ with intermediate radar backscatter, and sites 1 and 4 with the lowest biomass were located in areas with the lowest radar backscatter. In IFC_2, although site 3 showed significantly greater productivity in terms of LAI, biomass, and height, it was located in the same HZ as site 2. Saturation of the radar signal is believed to be the factor resulting in sites 2 and 3 being within the same HZ. The LAI and height of the corn plants at site 2 were approaching values known to cause saturation of the radar signal, and crop LAI and height at site 3 exceeded these values.

At the field level, delineation into three zones in IFC_1 resulted in a reduction in variance for EC_{30} and EC_{100} by 30% and 20%, respectively, with the 35° incident angle and 50% and 30%, respectively, with the 55° incident angle. The reduction in variance for LAI and yield was slightly higher at the shallower incident angle (30% and 20%, respectively) than at the steeper incident angle (10% for both). In IFC_2, the reduction in variance for any descriptor was only 10%. On a field basis, the HZ with the lowest radar backscatter was associated with the lowest productivity (**Table 6**). The mean LAI in IFC_1 at the 55° incident angle significantly increased from HZ_1 to HZ_3, as did radar backscatter. The EC_{30} and EC_{100} did not increase from HZ_2 to HZ_3. At the 35° incident angle, there was a significant difference in EC_{30} and LAI with HZ, and the radar backscatter increased from HZ_1 to HZ_3. Yield did not differ between HZ_1 and HZ_2 and between HZ_2 and HZ_3. The classifications were conducted during the early part of the growing season (up to 19 July 2001) prior to a rain-deficit period, whereas the harvest took place almost 3 months later. As yield results from a complex interaction of soil, climate, and vegetation, it could not be related to the HZs delineated prior to the rain deficit. Despite the lack of a relationship with yield, the delineation of HZ provides valuable information that can be used in optimizing inputs in areas of maximum potential production.

Wheat (F_{25})

Visual examination of the various SAR images shows that in IFC_1 there was no distinct spatial variation in the radar signal across F_{25} (**Figure 1**). In IFC_2 and more particularly IFC_3, spatial variation in the radar signal could be detected, more so with respect to the linear than the circular polarizations. Evidence of within-field spatial patterns only later in the season (IFC_2 and IFC_3) is consistent with previous observations

Table 7. Correlations (*r*) between C-band linear and circular copolarized and cross-polarized radar backscatter from wheat (F_{25}) for the image acquired at the 55° incident angle.

	HH	VV	HV	RR	LL	RL
IFC_1						
HH		0.46	0.26	0.46	0.38	**0.78**
VV			0.22	0.26	0.30	**0.76**
HV				0.60	0.65	0.15
RR					0.55	ns
LL						ns
RL						
IFC_2						
HH		ns	0.32	0.60	0.43	0.67
VV			–0.30	0.27	0.38	0.57
HV				0.43	0.26	ns
RR					0.45	0.28
LL						ns
RL						
IFC_3						
HH		ns	ns	0.64	0.55	0.51
VV			0.38	0.33	0.35	0.61
HV				0.35	0.19	0.40
RR					0.65	0.26
LL						0.15
RL						

Note: Significance values above the user-defined threshold of 0.70 are in bold. ns, not significant correlations at P = 0.05.

Table 8. Correlations (*r*) between C-band linear and circular copolarized and cross-polarized radar backscatter from wheat (F_{25}) for the image acquired at the 35° incident angle.

	HH	VV	HV	RR	LL	RL
IFC_1						
HH		0.47	0.26	0.32	0.39	**0.84**
VV			ns	ns	0.22	**0.81**
HV				0.62	**0.70**	0.14
RR					0.42	ns
LL						0.20
RL						
IFC_3						
HH		ns	ns	0.40	0.51	0.66
VV			0.23	ns	ns	0.55
HV				0.38	0.30	ns
RR					0.38	ns
LL						ns
RL						

Note: Significance values above the user-defined threshold of 0.70 are in bold. ns, not significant relationships at P = 0.05.

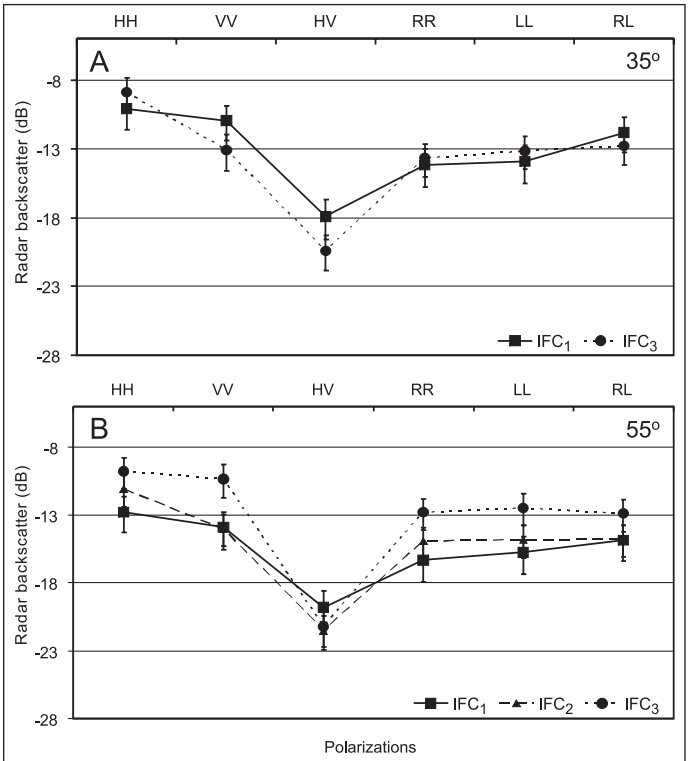

Figure 4. Seasonal changes in the C-band mean radar backscatter with its associated standard error (vertical bars) of wheat in F_{25}: (A) 35° incident angle; (B) 55° incident angle.

(McNairn et al., 2004). Further, McNairn et al. (2004) indicated that HV and VV polarizations appeared more sensitive to within-field variability in wheat than HH, RR, LL, and RL. In this study, on a whole-field basis, no significant change in the mean backscatter value for the wheat field was evident at either incident angle or in any polarization from IFC_1 through to IFC_3 (**Figure 4**).

Statistical analyses indicated substantially lower correlations between polarizations for wheat than for corn in all IFCs (**Tables 7 and 8**). The strongest correlations were evident in IFC_1, regardless of incident angle, between the linear copolarization (HH and VV) and circular cross-polarization (RL) (r = 0.76–0.81) and between the circular copolarization (RR and LL) and linear cross-polarizations (HV) (r = 0.60–0.70). As the season progressed and the wheat matured, however, the strength of the relationship between these polarizations decreased. The relationships between all other polarizations were weak, suggesting that different information may be obtained using the different polarizations.

The correlation results reported for both the cornfield and wheat field indicate that when biomass increases, correlations among polarization responses decrease. Early in the season, single scattering dominates like copolarizations and circular cross-polarizations; later in the season as the canopy closes and biomass increases, direct scattering from within the canopy dominates the responses associated with these polarizations. The components within the canopy to which the incident vertical or horizontal wave interacts will be different due to the orientation of the wave and the canopy structure. Wheat has a

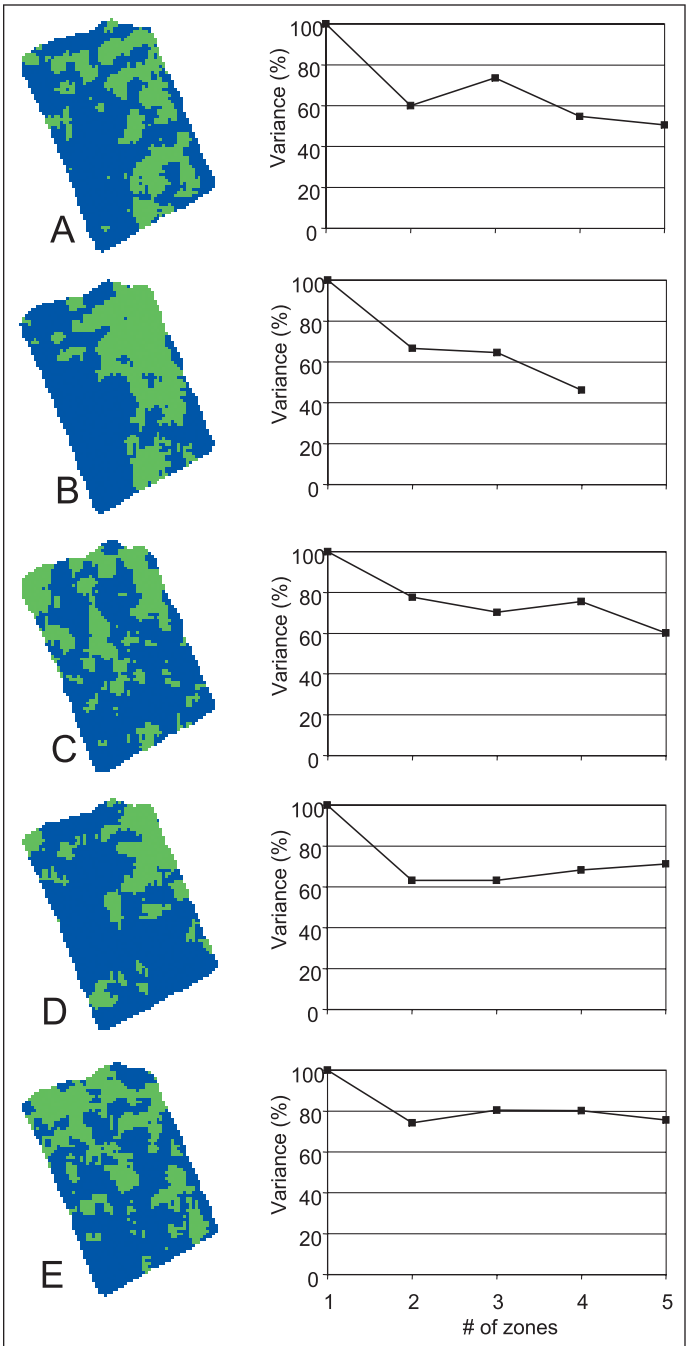

Figure 5. Fuzzy K-mean classified images for field F_{25} showing two zones derived from polarized C-band airborne radar acquired at the 35° incident angle: (A) HH in IFC_1, (B) HV in IFC_1, (C) HV in IFC_3, (D) VV in IFC_1, and (E) VV in IFC_3.

very pronounced vertical structure, and thus the lower correlation between backscatter from horizontal and vertical polarizations, relative to the corn canopy, can be explained. Early in the season, or for lower biomass canopies, repolarization of the linear or circular waves will be due to multiple scattering between the soil and canopy, as well as within the canopy itself. As biomass increases, volume scattering due to multiple interactions within the canopy itself will dominate the response of HV, VH, RR, and RL

Table 9. Mean (±SE) backscatter values (dB) for the zones in the wheat field (F_{25}) derived from the 35° incident angle imagery.

Polarization	Zone	IFC_1	IFC_3
HH	1	–10.4±0.1b	—
	2	–9.3±0.1a	—
HV	1	–18.3±0.1b	–20.9±0.1b
	2	–17.2±0.1a	–19.9±0.2a
VV	1	–11.2±0.1b	–13.2±0.1b
	2	–10.3±0.1a	–12.5±0.2a

Note: Means within a column followed by the same letter are not significantly different at $P = 0.05$.

polarizations. The complexity of the crop canopy, in general, increases as the canopy matures, and thus scattering from the canopy volume could be expected to be less consistent among incident waves.

The results for zone delineation within F_{25} using fuzzy K-means analyses differed with the radar polarization. Assuming that the difference in mean backscatter between HZs must exceed the calibration accuracy of 0.8 dB, no more than three HZs could be delineated regardless of polarization, incident angle, or date. HH was ineffective in delineating HZs except in IFC_1 with the 35° incident angle. In this particular case, two HZs reduced backscatter variance by 40%. The mean backscatter of HZ_1 was 1.07 dB higher than that of HZ_2. At the 35° incident angle, with both VV and HV polarizations, two HZs were appropriate. With three or more zones, either no further reduction in variance was observed or the difference in mean backscatter values among zones was less than 0.8 dB (**Figure 5**; **Table 9**). With respect to the 55° incident angle, regardless of the date, two HZs were delineated in F_{25} using the VV polarization (**Figure 6**; **Table 10**). Although in both IFC_2 and IFC_3, the reduction in variance was noticeably greater with three HZs (40%–50% compared with 25%–30%), the difference in the mean backscatter values for HZ_1 and HZ_2 of 0.7 dB was less than the calibration accuracy. No zone delineation was evident with the 55° incident angle HV image in IFC_1, but F_{25} could be delineated into three HZs using the HV imagery in both IFC_2 and IFC_3. The reduction in variance of backscatter was 50%, and the mean backscatter values differed by 0.82–1.90 dB (**Figure 7**; **Table 10**). The improvement in within-field zone delineation using the VV and HV polarizations was not unexpected, as vertically polarized waves are both scattered and attenuated by the vertical structures in wheat (Picard et al., 2003) and thus provide more information than horizontally polarized waves. Further, increased ability to map crop type and condition with RADARSAT-2 is anticipated due to the presence of VV and HV polarizations (van der Sanden, 2004). Visually, the inclusion of dual linear polarizations, all three linear polarizations, or all three linear plus the circular polarizations did not appear to alter the HZ delineation patterns compared with the individual linear polarizations. Combining HV with HH or HV with VV

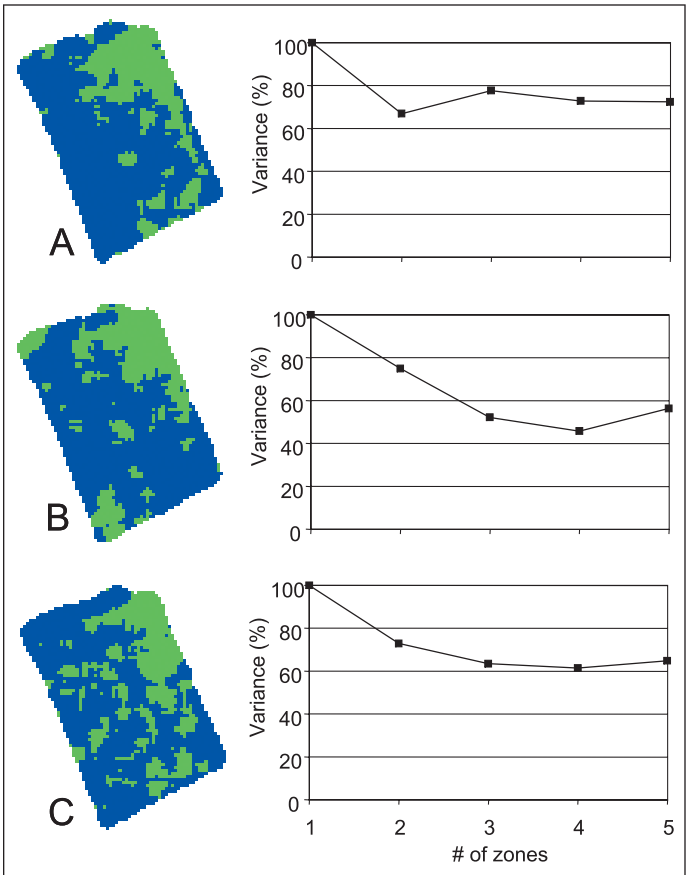

Figure 6. Fuzzy K-mean classified images for field F_{25} showing two zones derived from VV-polarized C-band airborne radar acquired at the 55° incident angle in (A) IFC_1, (B) IFC_2, and (C) IFC_3.

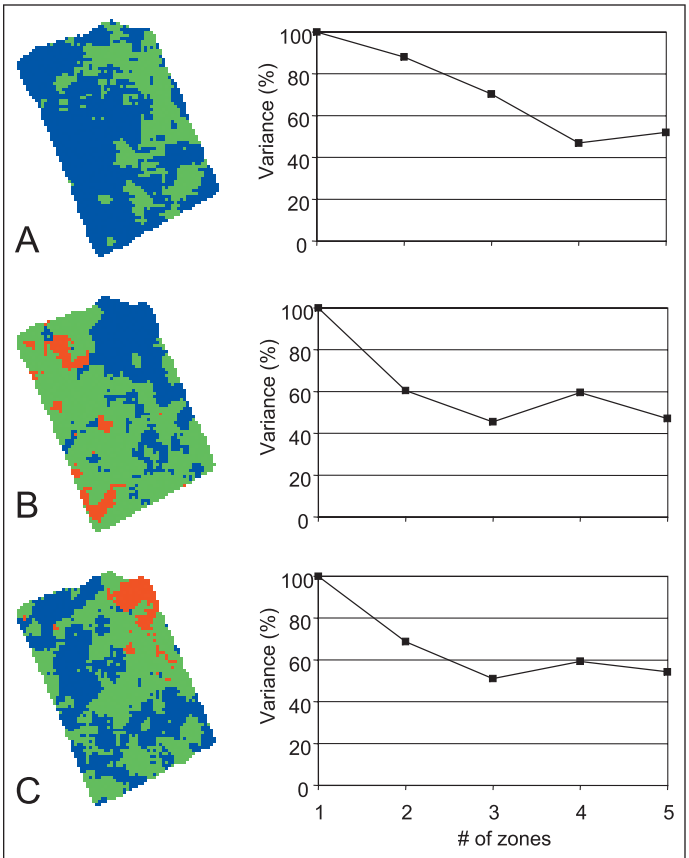

Figure 7. Fuzzy K-mean classified images for field F_{25} showing two and three zones derived from HV-polarized C-band airborne radar acquired at the 55° incident angle in (A) IFC_1, (B) IFC_2, and (C) IFC_3.

Table 10. Mean (±SE) backscatter values (dB) for the zones in the wheat field (F_{25}) derived from the 55° incident angle imagery.

Polarization	Zone	IFC_1	IFC_2	IFC_3
HV	1	—	–22.4±0.1c	–23.0±0.2c
	2	—	–21.4±0.1b	–22.2±0.1b
	3	—	–19.7±0.4a	–20.3±0.7a
VV	1	–14.3±0.1b	–14.4±0.1b	–11.6±0.1b
	2	–13.4±0.1a	–13.4±0.2a	–10.7±0.2a

Note: Means within a column followed by the same letter are not significantly different at $P = 0.05$.

did not alter the HZ pattern evident with the single HH or VV polarization, respectively. The results for the three linear polarizations were similar to those with the three linear polarizations in combination with the three circular polarizations, both of which were the same as with VV alone.

The northeast corner of F_{25} was consistently delineated as a zone of higher backscatter with the VV imagery; in the case of HV, this area showed highest backscatter in IFC_1 and IFC_3 relative to the rest of the field but lower backscatter in IFC_2. The soil in this area of F_{25} is imperfectly drained, whereas that of the remainder of F_{25} is poorly drained (Marshall et al., 1979; Figure 1 in Liu et al., 2005) and likely affected plant growth.

In an earlier study, within-field variation in wheat radar backscatter was dependent on variation in wheat head emergence and could not be seen early in the season during vegetative growth or late in the season when the crop is fully senesced (McNairn et al., 2004). In the current study, wheat was in the green vegetative growth phase in IFC_1 while heading was evident in IFC_2. The plant phenological and biophysical data collected from the seven sampling sites in the field indicated that the degree of heading varied across the field (**Table 11**). In the northeast corner of field F_{25}, at sites 1 and 2, the wheat was more advanced, with one half of the heads emerged compared with the onset of heading at the other five sites; the biomass attributable to the heads at sites 1 and 2 was also significantly greater than that at the other five sites. In IFC_3, at sites 1 and 2 and at site 7 in the southeast corner of F_{25}, the wheat heads were at the milky stage and beginning to undergo senescence compared to the green empty head at the other four sites located on the west side of the field. These data support the hypothesis that later in the growing season, backscatter is a function of the canopy structure, in particular the heads, which are the most significant biomass and moisture component (McNairn et al., 2004).

Table 11. Wheat biophysical descriptors measured at select sample sites in IFC_1, IFC_2, and IFC_3.

	LAI		Fresh biomass ($kg \cdot m^{-2}$)			
Sample site	Green	Total	Green leaf + stem	Senescing leaf	Head	Plant height (cm)
IFC_1						
1	3.70a	3.81a	3.191a	—	—	50a
2	3.16a	3.16a	1.546b	—	—	38b
3	0.74c	0.75c	0.429c	—	—	16d
4	1.85b	1.85b	0.820bc	—	—	31bc
5	1.32bc	1.32bc	0.700bc	—	—	—
6	0.82c	0.82c	0.464c	—	—	23cd
7	1.22bc	1.22bc	0.650bc	—	—	26cd
SE			0.337	—	—	
IFC_2						
1	2.52ab	2.78ab	2.404a	0.085a	0.392ab	113a
2	3.44a	3.59a	2.824a	0.045b	0.436a	98a
3	1.84b	1.86b	1.303a	0.004c	0.105c	49c
4	2.97ab	3.01ab	2.295a	0.021bc	0.190bc	61bc
5	2.72ab	2.78ab	2.195a	0.027bc	0.140c	54bc
6	2.67ab	2.75ab	2.138a	0.032bc	0.243bc	54bc
7	2.92ab	2.97ab	2.416a	0.020bc	0.310abc	71b
SE			0.365	0.011	0.077	
IFC_3						
1	0.65d	1.61bc	1.680bc	0.106a	1.117b	116a
2	1.75a	2.76a	2.655a	0.117a	1.628a	108b
3	1.34b	1.54bcd	1.687bc	0.033cd	0.388c	95de
4	1.11bc	1.31cd	1.418c	0.023d	0.424c	102bc
5	0.90cd	1.19d	1.413c	0.041cd	0.503c	97d
6	1.13bc	1.48cd	1.516bc	0.052c	0.883b	90e
7	1.39b	1.88b	1.947b	0.074b	0.970b	97cd
SE			0.160	0.008	0.117	

Note: Means within a column followed by the same letter are not significantly different at $P = 0.05$.

In terms of soil and plant descriptors measured at the field level, HZ_2 was generally found to have lower electrical conductivity and higher yield. With respect to LAI, the date of IFC influenced the zone in which LAI was highest. In IFC_1, regardless of polarization, the zone with higher LAI was also the zone of higher backscatter, whereas in IFC_2 and IFC_3 the LAI was either not significantly different between zones or was higher in the lower backscatter HZ (**Table 12**). The wheat in the northeast corner of F_{25} was more phenologically advanced in all IFCs. In the IFC_2 VV image, the areas delineated as HZ_2 also contained a sloping area in the northwest corner and a nitrogen-deficient area in the southwest corner. Both of these areas showed earlier heading of the wheat plants compared to all other areas of the field, likely due to the stress incurred from low nitrogen and being on a downward slope. The HV-delineated zones showed some interesting differences between IFC_2 and IFC_3. In IFC_2, in the northeast corner where LAI was highest, backscatter was lowest, whereas this same area in IFC_3 exhibited the lowest LAI and highest backscatter (**Table 12**). Again, these differences reflected senescence onset in the most advanced areas (i.e., northeast corner).

Conclusions

Traditionally, producers manage uniformly each agricultural field, applying inputs at a single rate. There is increasing recognition that within-field spatial variability exists and that remote sensing can be used to map this variability to achieve more sustainable management practices. To date, investigations have largely focused on optical remote sensing, but cloud cover often precludes the acquisition of timely imagery. Previous studies indicated SAR imagery could be useful in zone delineation. Only a single date of imagery was available, however, and thus the focus of this study was to investigate when in the growing season can information on crop condition be derived from radar backscatter.

Three imagery dates (early, mid, and late season) at two incidence angles (35° and 55°) were acquired in this study. The results confirmed that SAR can be used to delineate zones of

Table 12. Relationship between zone delineation using HV- and VV-polarized radar and soil electrical conductivity (EC_{30} and EC_{100}) and field-scale wheat biophysical descriptors (F_{25}).

Field campaign	Incident angle (°)	Zone	EC_{30} (mS)	EC_{100} (mS)	LAI[a]	Yield ($kg \cdot m^{-2}$)
HV polarization						
IFC_1	35	1	18.58±0.55a	25.31±0.65a	1.30±0.13b	3.56±0.07b
		2	15.93±0.99b	23.11±1.17b	1.98±0.23a	3.93±0.13a
IFC_2	55	1	15.24±0.78b	21.58±0.90b	3.02±0.13a	3.90±0.10a
		2	19.22±0.54a	26.30±0.62a	2.19±0.09b	3.55±0.07b
		3	19.66±3.41ab	25.87±3.94a	1.34±0.54b	2.69±0.45b
IFC_3	55	1	19.41±0.55a	26.51±0.68a	1.39±0.06a	3.52±0.08b
		2	17.54±0.56b	24.14±0.69b	1.26±0.06a	3.68±0.08b
		3	8.01±1.72c	14.49±2.10c	1.11±0.18a	4.55±0.25a
VV polarization						
IFC_1	55	1	19.67±0.48a	26.19±0.58a	1.12±0.11b	3.54±0.07b
		2	14.47±0.71b	21.46±0.86b	2.44±0.16a	3.99±0.10a
IFC_2	55	1	19.22±0.50a	25.89±0.57a	2.42±0.09b	3.57±0.07b
		2	14.44±0.86b	21.11±0.99b	2.87±0.15a	4.03±0.12a
IFC_3	55	1	18.97±0.44a	25.87±0.56a	1.30±0.05a	3.54±0.07b
		2	13.45±0.87b	20.24±1.13b	1.19±0.10b	4.06±0.14a

Note: Means within a column followed by the same letter are not significantly different at $P = 0.05$.
[a]Derived from CASI measurements.

productivity within an agricultural field. However, the timing of the radar data acquisition and the inherent variability in the soil within the fields are key to the successful extraction of information and varies with the crop being investigated. In corn, saturation of the C-band radar signal, at a relatively early stage in the development of the canopy, limits its use, and in wheat the onset of heading appears to be an influential factor in detecting homogeneous zones. All linear and circular polarizations in the high-pedodiversity cornfield showed similar results with respect to HZ delineation, and in the lower pedodiversity wheat field HV and VV appeared to be most useful. Single polarizations were as effective as two or three linear polarizations. The addition of the circular polarizations to the linear polarizations did not affect zone delineation and did not enhance the ability to define zones of productivity. The use of shallow incident angles appears to be more effective in providing plant information than steeper incident angles. C-band SAR imagery can provide some capability in delineating homogenous zones of growth to support site-specific agriculture. The results suggest that the launch of RADARSAT-2, in which multiple polarizations will be available compared to the single polarization (HH) on RADARSAT-1, may increase the opportunity to use radar for HZ delineation and spatial management of agricultural fields.

Acknowledgements

This study was funded by the Government Related Initiatives Program (GRIP) project between the Canadian Space Agency and Agriculture and Agri-Food Canada. The authors thank Lynda Blackburn, Dave Dow, Dave Meredith, Matt McKechnie, Ian Fox, and Anna Pacheco for collecting and processing the data, and Drs. Ian Strachan and Klaus Hochheim for contributing to the experimental design. This is LRC contribution number 38705054 and ECORC contribution number 05-584.

References

Brisco, B., Brown, R.J., Hirose, T., McNairn, H., and Staenz, K. 1998. Precision agriculture and the role of remote sensing: a review. *Canadian Journal of Remote Sensing*, Vol. 24, No. 3, pp. 315–327.

Bugden, J., McNairn, H., and Pattey, E. 2003. Procedures for end-users to assess SAR image quality. In *Proceedings of the 5th Advanced SAR (ASAR) Workshop*, 25–27 June 2003, St. Hubert, Que. Canadian Space Agency, St. Hubert, Que. CD-ROM.

Chen, F., Kissel, D.E., West, L.T., and Adkins, W. 2000. Field-scale mapping of surface soil organic carbon using remotely sensed imagery. *Soil Science Society of America Journal*, Vol. 64, No. 2, pp. 746–753.

Doerge, T. 1999. Defining management zones for precision farming. *Crop Insights*, Vol. 8, No. 21, pp. 1–5.

Ferrazzoli, P., Paloscia, S., Pampaloni, P., Schiavon, G., Sigismondi, S., and Solimini, D. 1997. The potential of multifrequency polarimetric SAR in assessing agricultural and arboreous biomass. *IEEE Transactions on Geoscience and Remote Sensing*, Vol. 35, No. 1, pp. 5–17.

Fleming, K.L., Westfall, D.G., Wiens, D.W., and Brodahl, M.C. 2000. Evaluating farmer defined management zone maps for variable rate fertilizer application. *Precision Agriculture*, Vol. 2, pp. 201–215.

Frazier, B.E., Walters, C.S., and Perry, E.M. 1997. Role of remote sensing in site-specific management. In *The state of site-specific management for agriculture*. Edited by F.J. Pierce and E.J. Sadler. ASA–CSSA–SSSA, Inc., Madison, Wisc. pp. 149–160.

Fridgen, J.J., Kitchen, N.R., and Sudduth, K.A. 2000. Variability of soil and landscape attributes within sub-field management zones. In *Proceedings of the 5th International Conference on Precision Agriculture*, 16–19 July 2000, Bloomington, Mn. Edited by P.C. Robert, R.H. Rust, and W.E. Larson. ASA–CSSA–SSSA, Madison, Wisc. CD-ROM.

Haboudane, D., Miller, J.R., Pattey, E., Zarco-Tejada, P.J., and Strachan, I.B. 2004. Hyperspectral vegetation indices and novel algorithms for predicting green LAI of crop canopies: modeling and validation in the context of precision agriculture. *Remote Sensing of Environment*, Vol. 90, pp. 337–352.

Hawkins, R.K., Touzi, R., Wind, A., Murnagham, K., and Livingstone, C.E. 1999. Polarimetric calibration results and error budget for SAR-580 system. In *Proceedings of the CEOS'99 Working Group Workshop*, 26–29 October 1999, Toulouse, France. Edited by R.A. Harris and L. Ouwehand. ESA Publications Division, Noordwijk, The Netherlands, ESA Publication SP-450. Available from http://www.estec.esa.nl/ceos99/papers/p101.pdf.

Liu, J., Miller, J.R., Haboudane, D., Pattey, E., and Nolin, M.C. 2005. Variability of seasonal CASI image data products and potential application for management zone delineation for precision agriculture. *Canadian Journal of Remote Sensing*, Vol. 31, No. 5, pp. 400–411.

Lu, Y.-C., Daughtry, C., Hart, G., and Watkins, B. 1997. The current state of precision farming. *Food Reviews International*, Vol. 13, No. 2, pp. 141–162.

Marshall, I.B., Dumanski, J., Huffman, E.C., and Lajoie, P. 1979. *Soils capability and land use in the Ottawa urban fringe*. Land Resource Research Institute, Agriculture Canada, Ottawa, Ont. 59 pp.

McNairn, H., and Brisco, B. 2004. The application of C-band polarimetric SAR for agriculture: a review. *Canadian Journal of Remote Sensing*, Vol. 30, No. 3, pp. 525–542.

McNairn, H., Brown, R.J., McGovern, M., Huffman, T., and Ellis, J. 2000. Integration of multi-polarized SAR data and high spatial optical imagery for precision farming. In *Proceedings of the 22nd Canadian Symposium on Remote Sensing*, 21–25 August 2000, Victoria, B.C. Canadian Aeronautics and Space Institute (CASI), Ottawa, Ont. Available from http://ess.nrcan.gc.ca/esic/ccrspub-cctpub/pdf/4816.pdf.

McNairn, H., Deguise, J.-C., Secker, J., and Shang, J. 2001. Development of remote sensing image products for use in precision farming. In *ECPA 2001: Proceedings of the 3rd European Conference on Precision Agriculture*, 18–20 June 2001, Montpellier, France. Edited by G. Grenier and S. Blackmore. Agro-Montpellier, Montpellier, France. CD-ROM.

McNairn, H., Decker, V., and Murnagha, K. 2002. The sensitivity of C-band polarimetric SAR to crop condition. In *IGARSS 2002, Proceedings of the International Geoscience and Remote Sensing Symposium and 24th Canadian Symposium on Remote Sensing*, 24–28 June 2002, Toronto, Ont. IEEE, Piscataway, N.J. CD-ROM.

McNairn, H., Hochheim, K., and Rabe, N. 2004. Applying polarimetric radar imagery for mapping the productivity of wheat crops. *Canadian Journal of Remote Sensing*, Vol. 30, No. 3, pp. 517–524.

Moran, M.S., Inoue, I., and Barnes, E.M. 1997. Opportunities and limitations for image based remote sensing in precision crop management. *Remote Sensing of Environment*, Vol. 61, No. 3, pp. 319–346.

Morgenthaler, G.W., Khatib, N., and Kim, B. 2003. Incorporating a constrained optimization algorithm into remote sensing agriculture methodology. *Acta Astronautica*, Vol. 53, pp. 429–437.

Mulla, D.J., and Schepers, J.S. 1997. Key processes and properties for site-specific soil and crop management. In *The state of site-specific management for agriculture*. Edited by F.J. Pierce and E.J. Sadler. ASA–CSSA–SSSA, Inc., Madison, Wisc. pp. 1–18.

Mulla, D.J., Beatty, M., and Sekely, A.C. 2001. Evaluation of remote sensing and targeted soil sampling for variable rate application of nitrogen. In *Proceedings of the 5th International Conference on Precision Agriculture*, 16–19 July 2000, Bloomington, Mn. Edited by P.C. Robert, R.H. Rust, and W.E. Larson. ASA–CSSA–SSSA, Inc., Madison, Wisc. CD-ROM.

Perron, I., Nolin, M.C., Pattey, E., Bugden, J.L., and Smith, A. 2003. Comparaison de l'utilisation de la conductivite électrique apparente (CEa) des sols et des donnees polarimetriques RSO pour delimeter des unites d'amenagement agricole. In *Proceedings of the 25th Canadian Symposium on Remote Sensing – 11e Congrès de l'Association québécoise de télédétection*, 14–16 October 2003, Montréal, Que. Canadian Aeronautics and Space Institute (CASI), Ottawa, Ont. CD-ROM.

Picard, G., Le Toan, T., and Mattia, F. 2003. Understanding C-band radar backscatter from wheat canopy using a multiple-scattering coherent model. *IEEE Transactions on Geoscience and Remote Sensing*, Vol. 41, pp. 1583–1591.

Pierce, F.J., and Nowak, P. 1999. Aspects of precision agriculture. *Advances in Agronomy*, Vol. 67, pp. 1–85.

SAS Institute Inc. 1999. *SAS/STAT user's guide, version 8*. SAS Institute Inc., Cary, N.C.

Seelan, S.K., Laguette, S., Casady, G.M., and Seielstad, G.A. 2003. Remote sensing application for precision agriculture: a learning community approach. *Remote Sensing of Environment*, Vol. 88, No. 1–2, pp. 157–169.

Stafford, J.V. 2000. Implementing precision agriculture in the 21st century. *Agriculture Engineering and Research*, Vol. 76, pp. 267–275.

van der Sanden, J.J. 2004. Anticipated applications potential of RADARSAT-2 data. *Canadian Journal of Remote Sensing*, Vol. 30, No. 3, pp. 369–379.

Yang, C., and Anderson, G.L. 2000. Mapping grain sorghum yield variability using airborne digital videography. *Precision Agriculture*, Vol. 2, pp. 7–23.